

# Catalysis Science & Technology

Accepted Manuscript



This is an *Accepted Manuscript*, which has been through the Royal Society of Chemistry peer review process and has been accepted for publication.

*Accepted Manuscripts* are published online shortly after acceptance, before technical editing, formatting and proof reading. Using this free service, authors can make their results available to the community, in citable form, before we publish the edited article. We will replace this *Accepted Manuscript* with the edited and formatted *Advance Article* as soon as it is available.

You can find more information about *Accepted Manuscripts* in the [Information for Authors](#).

Please note that technical editing may introduce minor changes to the text and/or graphics, which may alter content. The journal's standard [Terms & Conditions](#) and the [Ethical guidelines](#) still apply. In no event shall the Royal Society of Chemistry be held responsible for any errors or omissions in this *Accepted Manuscript* or any consequences arising from the use of any information it contains.

## ARTICLE

# Catalytic mechanism of BsDyP an A-type dye-decolourising peroxidase: neither aspartate nor arginine is individually essential for peroxidase activity

Cite this: DOI: 10.1039/x0xx00000x

Received 00th January 2012,  
Accepted 00th January 2012

DOI: 10.1039/x0xx00000x

www.rsc.org/

S. Mendes,<sup>a</sup> T. Catarino,<sup>a,b</sup> C. Silveira,<sup>a</sup> S. Todorovic<sup>a</sup> and L.O. Martins<sup>a</sup>

BsDyP from *Bacillus subtilis* belongs to the new dye-decolourising peroxidase (DyP) family. Here we use transient kinetics to provide details on the catalytic cycle of BsDyP. The reaction of BsDyP with H<sub>2</sub>O<sub>2</sub> exhibits saturation behaviour consistent with a two-step mechanism involving the formation of an E-H<sub>2</sub>O<sub>2</sub> intermediate ( $K_1 = (12 \pm 1) \times 10^{-6}$  M) followed by formation of Compound I ( $k_1 = 22 \pm 1$  s<sup>-1</sup>). We demonstrate that the  $k_{1\text{obs}}$  is pH-dependent and controlled by an ionisable group with a pK<sub>a</sub> of 4.3 suggesting the involvement of distal Asp. The reaction of Compound I with guaiacol obeys second order kinetics ( $k_3' = (0.21 \pm 0.01) \times 10^6$  M<sup>-1</sup>s<sup>-1</sup>) while the reaction of Compound II with guaiacol shows saturation kinetics ( $K_4 = 22 \pm 5) \times 10^{-6}$  M and  $k_4 = 0.13 \pm 0.01$  s<sup>-1</sup>) and is the rate-limiting step in the BsDyP catalytic cycle. We furthermore use transient and steady-state kinetics, spectroscopic and electrochemical approaches to investigate the role of distal Asp240, Arg339 and Asn244 and proximal Asp383 residues in BsDyP. All mutations of distal residues affect particularly the  $K_1$  (and  $K_m$ ) for H<sub>2</sub>O<sub>2</sub> leading to catalytic efficiencies ( $k_{\text{cat}}/K_m$ ) of only one to two orders of magnitude lower than in the wild type. Notably, a significant improvement in the catalytic efficiency for reducing substrates is observed in variants. We conclude that the Asp and Arg residues are important for the proper binding of H<sub>2</sub>O<sub>2</sub> to the haem but none is individually indispensable for promoting H<sub>2</sub>O<sub>2</sub> (de)protonation and O-O bond cleavage. The obtained kinetic data suggest an important role of the distal Asn in modulating the acid-base catalysis of BsDyP. Our findings contribute to the establishment of structural determinants of DyPs that underlie their mechanistic properties; this has implications for their potential in biotechnological applications and sheds more light on subfamily-dependent features of these enzymes.

## Introduction

DyP-type peroxidases (DyPs) oxidize a remarkably wide range of substrates, from synthetic dyes and aromatic sulphides to phenolic and nonphenolic lignin compound units, lignin and even iron and manganese ions, using hydrogen peroxide as electron acceptor.<sup>1-5</sup> Some of DyPs represent, to a certain extent, the bacterial equivalent of fungal ligninolytic peroxidases (i.e. extracellular, class II peroxidases) due to their ability to oxidize high redox potential compounds.<sup>6-10</sup> DyPs have been classified into four phylogenetically distinct subfamilies on the basis of sequence comparison, with bacterial enzymes constituting A-C subfamilies and fungal enzymes belonging to D subfamily.<sup>1, 2, 4, 5, 11</sup> Class A contains enzymes with a Tat-dependent signal sequence, which indicates that they function

outside the cytoplasm, in the periplasm of Gram (-) bacteria or in the extracellular space, as is the case of *Bacillus subtilis* BsDyP.<sup>10, 12</sup> Classes B and C comprise (putative) cytoplasmic enzymes presumably involved in intracellular metabolism.<sup>4, 5</sup> Primary sequence and structural features of DyPs are unrelated to those of "classical" peroxidases; they show a typical ferredoxin-like fold, distinct from the motifs found in other haem peroxidases that have  $\alpha$ -helical structure.<sup>13-18</sup> DyPs lack the distal histidine; instead they house an aspartate residue proposed to take the role of the His in the enzymatic mechanism by acting as the acid-base catalyst that promotes the heterolytic cleavage of hydrogen peroxide to Compound I (Cpd I).<sup>19, 20</sup> A distal arginine paired with the histidine or aspartate is thought to be essential for proper coordination of the peroxide molecule at the haem site and stabilization of the Cpd I in classical peroxidases.<sup>19, 20</sup> The reaction of Cpd I with one equivalent of reducing substrate yields Compound II (Cpd II), which further reacts with a second equivalent of the reducing substrate yielding the resting state peroxidase. A limited number of biochemical and X-ray studies have addressed structural and functional aspects of DyPs, and many questions still remain unanswered.<sup>4, 5, 7, 15-18, 21-25</sup> Among them

<sup>a</sup> Instituto de Tecnologia Química e Biológica, Universidade Nova de Lisboa, Av. da República, 2780-157 Oeiras, Portugal E-mail: [lmartins@itqb.unl.pt](mailto:lmartins@itqb.unl.pt); phone: +351 214469534; Fax: +351 214411277.

<sup>b</sup> Departamento de Química, Faculdade de Ciências e Tecnologia, Universidade Nova de Lisboa, 2829-516 Caparica, Portugal

are those related to the details of the catalytic cycle, e.g. the mechanism of electron transfer to hydrogen peroxide, and oxidation of different substrates, crucial for understanding and exploring their catalytic properties. In DyPs a few mutagenesis studies have been employed in search of structural determinants of catalytic activity; the role of distal pocket residues in the formation of the Cpd I catalytic intermediate is particularly disputed and is currently the subject of intensive research.<sup>17, 18, 23</sup> Sugano *et al*<sup>23</sup> suggested that Asp acts as proton shuttle in the formation of Cpd I in *Bjerkandera adusta* D-type Dec1, while Arg stabilizes the negative charge during the heterolytic cleavage of the peroxide. Similarly, in the A-type enzyme from *Thermobifida fusca*, TfuDyP, substitution of Asp242 with Ala resulted in an inactive enzyme, pointing to a key role of the distal Asp in the catalytic mechanism.<sup>26</sup> The roles of the distal residues in the A-type EfeB/YcdB from *Escherichia coli* O157 seem more controversial; mutants D235A and R347E lose activity for guaiacol and catechol but, surprisingly, the distal D235N mutant keeps nearly the same activity for guaiacol as the wild type enzyme.<sup>18</sup> In the B-type bacterial *Rhodococcus jostii* RHA1 DypB and *Pseudomonas putida* MET94 PpDyP, the substitution of the conserved Arg, and not of the Asp, resulted in a significant drop in reactivity.<sup>12, 17</sup> This finding led to the proposal that a distal Arg acts as the acid-base catalyst in the Cpd I formation, through a mechanism that remains to be elucidated.<sup>12, 17</sup> It is not clear at this point whether the contradictory results regarding the role of the distal residues in the catalysis reflect differences in the mechanistic features of DyPs from different sources. Therefore, more systematic data on the thermodynamic and kinetic properties are needed to establish the structural determinants of DyPs catalytic mechanism.

Here we have investigated the catalytic cycle of A-type *B. subtilis* BsDyP and the impact of the substitution of three distal haem pocket residues, D240, R339 and N244, together with the proximal residue D383 (Fig. 1).<sup>12</sup> Transient kinetics was used to characterize BsDyP reaction with hydrogen peroxide and the reactivity of its Cpd I and Cpd II with guaiacol. The pH dependence of the reaction with hydrogen peroxide was investigated in detail. Site-directed mutagenesis has been used to construct variants and the effects of the substitutions were assessed by UV-visible and resonance Raman (RR) spectroscopies and cyclic voltammetry. Transient and steady state kinetics measurements revealed the catalytic properties of the variants and in particular the importance of the distal residues D240 and R339 in the catalytic cycle of BsDyP.

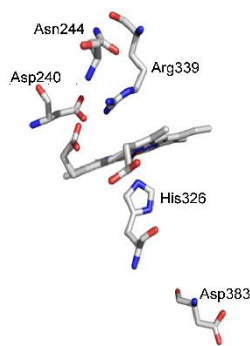


**Fig. 1** -The distal haem residues of BsDyP: Asp240, Arg339 and Asn244 in the model structure derived from the Phyre2 server.<sup>12</sup> On the proximal side, the haem iron is coordinated by H326 hydrogen bonded to Asp383.

## Results and discussion

### Reaction of BsDyP with hydrogen peroxide

The transient kinetics of BsDyP upon addition of 10  $\mu\text{M}$   $\text{H}_2\text{O}_2$  at pH 3.8, which is the optimal for activity<sup>12</sup>, reveal spectral changes that are indicative of Cpd I (Soret band with reduced intensity) (Fig. 2). These conditions lead to the formation of a stable Cpd I, with a  $t_{1/2}$  of  $\sim 3.6$  h; Cpd II is not observed even after addition of excess  $\text{H}_2\text{O}_2$  (50 molar equiv). The rates of Cpd I formation upon addition of increasing concentrations of  $\text{H}_2\text{O}_2$  were followed by measuring absorbance change at 397 nm, the isosbestic point of Cpd I and Cpd II (Fig. S1). All kinetic traces were of a single exponential character (Fig. S2).

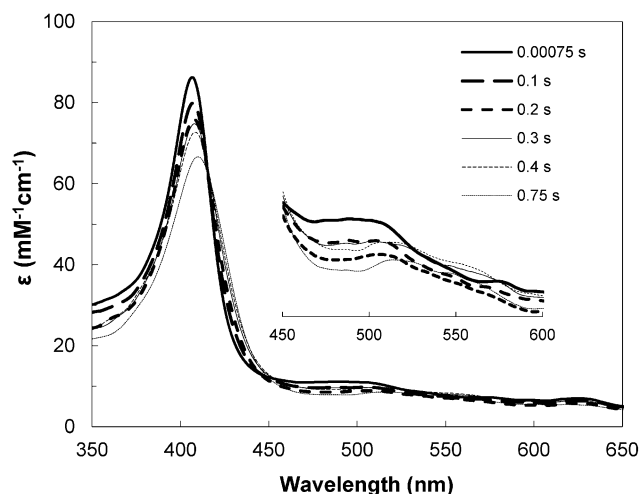
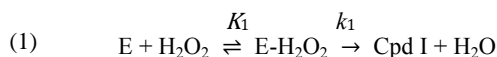


**Fig. 2.** Stopped-flow analysis of the reaction of BsDyP WT with  $\text{H}_2\text{O}_2$  in Britton-Robinson (BR) buffer, pH 3.8. The enzyme ( $\sim 2 \mu\text{M}$ ) was mixed with 5 equivalents of  $\text{H}_2\text{O}_2$  at  $25^\circ\text{C}$ . The time course spectra reveal the formation of an intermediate with the characteristics of Cpd I. The inset shows the enlarged region between 450 and 600 nm.

We have observed that rate constants for the formation of Cpd I ( $k_{\text{obs}}$ ) are linearly proportional to the  $\text{H}_2\text{O}_2$  concentration up to 10  $\mu\text{M}$ , whereas at higher concentrations saturation occurs (Fig. 3A and inset). This behaviour is consistent with a two-step mechanism as initially proposed by Poulos and Kraut.<sup>27</sup> Two essential features of this mechanism are the acid-base catalysis by a distal histidine (His-42 in cytochrome c peroxidase (CcP)) and charge stabilization of a precursor enzyme-substrate complex by the conserved arginine (Arg-38).<sup>27</sup> In the first step there is a pre-equilibrium of reactants to form a precursor complex  $\text{E-H}_2\text{O}_2$ , often called Compound 0<sup>19, 28</sup>, and in the second step the O-O bond is cleaved producing Cpd I and water:



where

$$(2) \quad K_1 = \frac{[\text{E}][\text{H}_2\text{O}_2]}{[\text{E-H}_2\text{O}_2]}$$

$$(3) \quad k_{\text{obs}} = \frac{k_1}{1 + \frac{K_1}{[\text{H}_2\text{O}_2]}}$$

in which  $K_1$  (M) is an apparent dissociation constant and  $k_1$  ( $s^{-1}$ ) is a first-order catalytic rate constant. The observation that the  $k_{1\text{obs}}$  vs.  $[H_2O_2]$  plot intersect the origin indicates that Cpd I formation is irreversible and justifies the omission of  $k_{-1}$  from equation 1. The constants  $K_1$  and  $k_1$ , calculated from equation (3), are  $(12 \pm 1) \times 10^{-6}$  M and  $22 \pm 1$   $s^{-1}$ . The kinetic evidence for a two-step mechanism in BsDyP is very interesting and surprising since in spite of the accumulated data supporting the Poulos-Kraut model<sup>19, 20</sup> the presence of an intermediate precursor of Cpd I, is suggested only by a few kinetic reports. These include low temperature studies on horseradish peroxidase (HRP)<sup>29-32</sup>, HRP variants<sup>33, 34</sup> and lactoperoxidase, using cryoradiolysis and RR spectroscopy.<sup>35</sup> The second order rate constant of Cpd I formation ( $k_1' = k_1 / K_1$ ),  $((1.8 \pm 0.1) \times 10^6$   $M^{-1} s^{-1}$ ) is of the same magnitude as those previously reported for the HRP,<sup>34, 36</sup> lignin and manganese peroxidase from the white-rot fungus *P. chrysosporium*<sup>37, 38</sup> and versatile peroxidase from *Pleurotus eryngii*<sup>39</sup> and it is one order of magnitude higher than that of bacterial DyPB from *R. jostii* RHA1.<sup>22</sup>

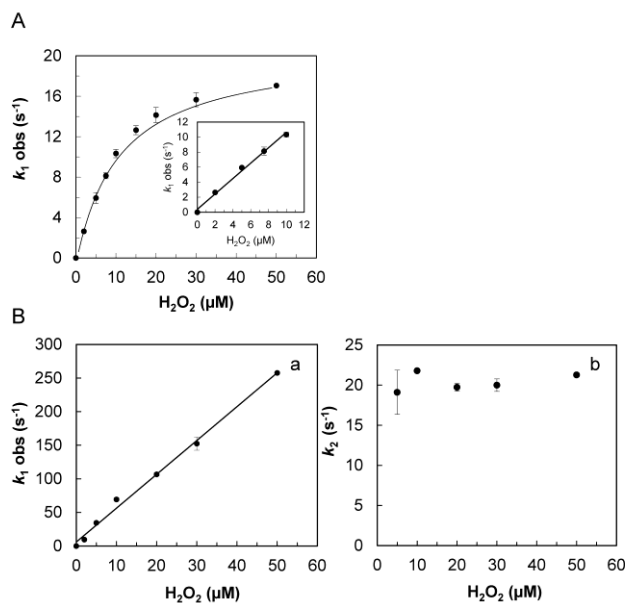


**Fig. 3** - Reaction of BsDyP WT with  $H_2O_2$  at pH 3.8 (A) and at pH 7 (B). Cpd I (A and B (a)) and Cpd II (B (b)) formation as a function of time were followed at 397 and 420 nm, respectively and the rate constants were obtained from single exponential fits (Fig. S2).

The plot of  $\log k_{1\text{obs}}$  vs. pH (Fig. 4 and Fig. S3) demonstrates that the rate of Cpd I formation increases with increasing pH. It is controlled by an ionisable group in the protein having a  $pK_a$  of 4.3 which is compatible with the distal Asp ( $pK_a$  3.9 for free Asp). This pH-dependence has been observed in peroxidases including HRP, chloroperoxidase and CcP where a ionisable residue with a  $pK_a$  from 3 to 5 was suggested to play a role in the deprotonation and O-O heterolytic cleavage of  $H_2O_2$ ;<sup>40</sup> lignin, manganese and versatile peroxidases, on the other hand, show a pH-independent Cpd I formation.<sup>37-39</sup>

At  $pH \geq 5$ , the observed spectral changes indicate Cpd I, followed by Cpd II formation, as judged by Soret band red shift from 407 to 418-420 nm and  $\alpha$  and  $\beta$  bands at 526 and 556 nm, respectively (Fig. 5

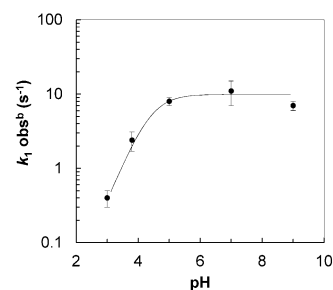


**Fig. 4** - pH dependence of Cpd I formation in reaction of BsDyP WT with  $H_2O_2$ . The line was calculated using the equation:  $k_{1\text{obs}} = k_{1\text{obs}}^b / (1 + [H^+]/K_a)$ , where  $k_{1\text{obs}}^b$  is the observed rate constant at high pH.

and data not shown). This is in accordance with previous reports that show the formation of a stable Cpd II intermediate upon addition of hydrogen peroxide to the resting state of BsDyP and DyPA from *R. jostii* RHA1 at  $pH \sim 7.5$ .<sup>12, 22</sup> We have investigated in detail the reaction of BsDyP with hydrogen peroxide at pH 7. The decay of Cpd I to Cpd II was followed at 420 nm, the isosbestic point of resting enzyme and Cpd I (Fig. S1).

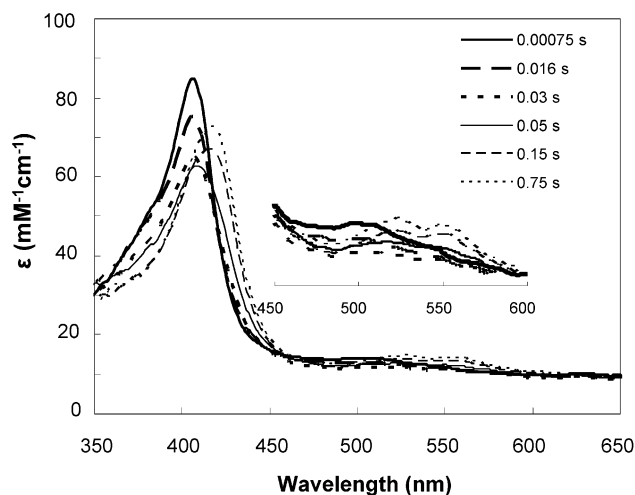
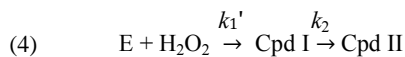


**Fig. 5**. Stopped-flow analysis of the reaction of BsDyP WT with  $H_2O_2$  in Britton-Robinson (BR) buffer, pH 7. The enzyme ( $\sim 2$   $\mu M$ ) was mixed with 10  $\mu M$   $H_2O_2$  at 25°C. The time course spectra reveal that formation of Cpd I is followed by an intermediate indicative of Cpd II. The inset shows the region between 450 and 600 nm.

We show that  $k_{1\text{obs}}$  is linearly proportional to the  $H_2O_2$  concentration up to 50-fold excess. The plot also intercepts the origin (Fig. 3B(a)), indicating that the Cpd I formation obeys second-order kinetics ( $k_1' = 10 \pm 3$   $M^{-1} s^{-1}$ ) and is essentially irreversible in accordance to kinetic scheme (4). The rate constant for the spontaneous decay of Cpd I to Cpd II ( $k_2 = 14 \pm 3$   $s^{-1}$ ) is independent of peroxide concentration (Fig. 3B (b)) showing that the decay of Cpd I to Cpd II is a unimolecular step. The rate constants for the formation and decay of Cpd I were calculated assuming the kinetic scheme (4)



Where the second order rate constant  $k_1'$  was calculated from the slope of Fig. 3 B(a) and  $k_2$  obtained directly from the exponential fit

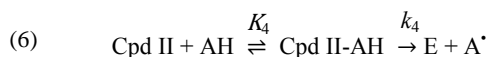
of the absorbance measured at 420 nm (Fig. S3 B). The spontaneous decay of Cpd I at pH 5 and 9 occurs at comparable rates ( $k_2 = 12 \pm 3 \text{ s}^{-1}$ ) (Fig. S3 B). The presence of excess of  $\text{H}_2\text{O}_2$  at pH 7, but not at pH 3.8, leads to spectral features indicative of Cpd III formation, as judged by Soret band at 414 nm and  $\alpha$  and  $\beta$  bands at 545 and 580 nm (Fig. S1 B). The observed pH-dependent decay of Cpd I to Cpd II in BsDyP contrasts the previously reported results on the B-type *R. jostii* RHA1 DyPB that show pH-independent spontaneous decay to Cpd II, and those on B-type *P. putida* MET 94 PpDyP where no decay to Cpd II was observed at pH 7.<sup>22, 41</sup>

### Reaction of Cpd I and Cpd II with guaiacol

In the next step, the catalytic reaction of BsDyP was followed at pH 3.8 in the presence of the reducing substrate guaiacol. Stopped-flow experiments were performed where Cpd I was generated from WT and  $\text{H}_2\text{O}_2$  (1:2) and reacted with guaiacol. Both the formation of Cpd II and its subsequent conversion to the resting enzyme in the presence of guaiacol was followed at 420 nm, the isosbestic point for Cpd I and resting enzyme (Fig. S1).<sup>40</sup> The biphasic curve (Fig. S4) shows an initial increase of absorbance (formation of Cpd II), which is completed in less than 150 ms and followed by a slower decline (reduction of Cpd II). The traces were exponential in character. The second order rate constant  $k_3'$  ( $0.21 \pm 0.01$ )  $\times 10^6 \text{ M}^{-1}\text{s}^{-1}$  was estimated from the slope of the plot in Fig. 6A assuming the kinetic scheme:



Saturation kinetics was observed in the reaction between Cpd II with guaiacol for concentrations  $\geq 0.1 \text{ mM}$  (Fig. 6B), indicating a pre-equilibrium binding of guaiacol prior to rate-limiting electron transfer of the following general form:



where

$$K_4 = \frac{[\text{Cpd II}][\text{AH}]}{[\text{Cpd II-AH}]}$$

$$(7) \quad k_{4\text{obs}} = \frac{k_4}{1 + \frac{K_4}{[\text{AH}]}}$$

The apparent dissociation constant,  $K_4$ , and the first order rate constant,  $k_4'$  for the reduction of Cpd II to the resting enzyme were calculated from equation (8) and found to be  $(22 \pm 5) \times 10^6 \text{ M}$  and  $0.13 \pm 0.01 \text{ s}^{-1}$ , respectively. The double reciprocal plot of the data is linear (data not shown). Saturation kinetics was previously described, e.g. for lignin peroxidase with veratryl alcohol<sup>42</sup>, manganese peroxidase with Mn(II)<sup>37</sup> and HRP with ABTS and o-diphenols<sup>43</sup>, and was attributed to a binding interaction between the enzyme and substrate, forming an enzyme-substrate complex, followed by the enzyme reduction. Following this analogy we propose here the same mechanism for BsDyP. The rate limiting step in the BsDyP catalytic reaction is the Cpd II reduction to the resting enzyme  $k_4'$  (calculated from  $k_4/K_4$ ) ( $5.9 \pm 0.1$ )  $\times 10^3 \text{ M}^{-1}\text{s}^{-1}$ , which is lower than  $k_3'$  ( $0.21 \pm 0.01$ )  $\times 10^6 \text{ M}^{-1}\text{s}^{-1}$  and  $k_1'$  ( $1.8 \pm 0.1$ )  $\times 10^6$

$\text{M}^{-1} \text{ s}^{-1}$ ), as typically observed in peroxidases.<sup>37, 42, 44</sup> Overall, the obtained results allow for the proposal of a catalytic cycle for BsDyP at pH 3.8 and pH 7 as shown in Fig. 7.

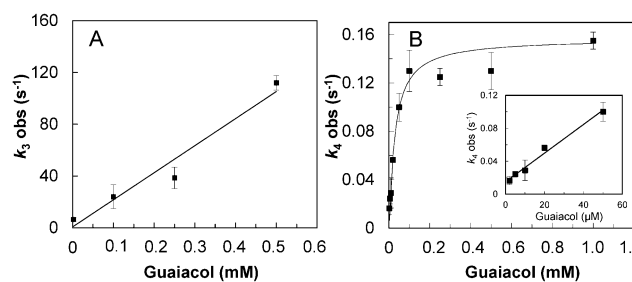


**Fig. 6** – Reaction of Cpd I (A) and Cpd II (B) with guaiacol at pH 3.8 followed by stopped flow. One syringe contained BsDyP WT mixed with  $\text{H}_2\text{O}_2$  (1:2) and the other contained guaiacol. Cpd II formation (A) and Cpd II decay to native enzyme (B) were followed at 420 nm (Fig. S4).

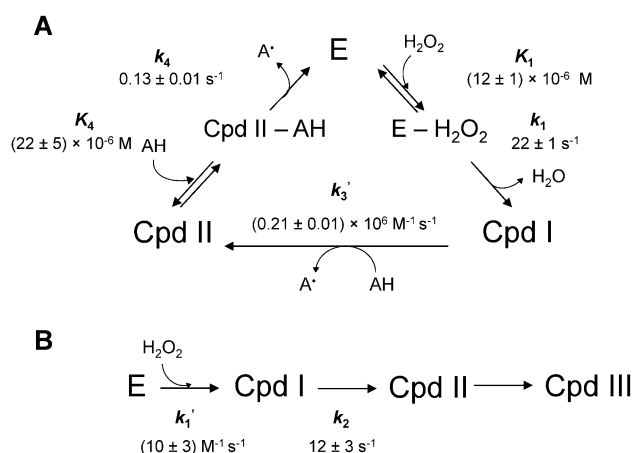


**Fig. 7** – Schematic representation of catalytic cycle of BsDyP (A) at pH 3.8, the optimal for activity and (B) at pH 7, where no catalytic activity for reducing substrates was detected (Fig. S5). The resting enzyme E, Cpd I, Cpd II and Cpd III intermediates were spectroscopically identified; the presence of intermediates E- $\text{H}_2\text{O}_2$  and Cpd II-AH is inferred from kinetic analysis. AH represents the reducing substrate and  $\text{A}^\bullet$  the radical product.

### Biochemical and spectroscopic characterization of BsDyP variants

The variants D240N, D383N, N244L, R339L and D240N-R339L (Fig. 1) showed a similar chromatographic pattern during purification to the BsDyP WT.<sup>12</sup> The protein purity was judged by SDS-PAGE which showed a single band at 48 kDa for all variants. They exhibited lower haem *b* content than the WT, as estimated by the pyridine ferrohemochrome method, with D240N being the most significantly haem-depleted (Table 1). The reasons behind the observed differences in protein yields and haem content among the variants are not clear at the moment, but we can hypothesize that the mutations affected the gene expression and/or led to instability of the produced proteins and haem binding. The Reinheitszahl value, which reflects the purity of haemoproteins, is  $\sim 2$  for BsDyP WT, N244L and D383N variants,  $\sim 1$  for D240N,  $\sim 3$  for R339L and D240N/R339L variant. The electronic absorption features of BsDyP variants at pH 7.6 reveal the characteristic Soret band at  $\sim 406 \text{ nm}$ , Q

bands at ~500, ~540 and ~570 nm, and a charge transfer (CT) band at ~630 nm, comparable to the WT enzyme (Fig. 8, Table 1) and similar to the values observed at acidic pH (data not shown). Small differences in the spectra indicate subtle perturbations of the respective active sites, which are most pronounced in the D240N and R339L variants.

**Table 1.** Spectroscopic and redox properties of BsDyP WT and variants.

	$\lambda_{\text{max}}$ (nm)	$\epsilon$ ( $\text{mM}^{-1}\text{cm}^{-1}$ )	Haem content	$E^{0'}$ (mV)
WT	407	$87 \pm 2$	$0.52 \pm 0.01$	$-40 \pm 4^*$
D240N	408	$39 \pm 2$	$0.08 \pm 0.01$	$-120 \pm 10$
R339L	406	$128 \pm 2$	$0.30 \pm 0.04$	$-105 \pm 20$
D240N-R339L	406	$113 \pm 3$	$0.19 \pm 0.01$	$-125 \pm 5$
N244L	406	$78 \pm 5$	$0.33 \pm 0.04$	$-83 \pm 8$
D383N	408	$117 \pm 32$	$0.21 \pm 0.04$	$-75 \pm 5$

\* 45

The structural features of the haem pocket of the studied variants were characterized in more detail by RR spectroscopy (Fig. 9). When excited into the Soret electronic transition band, RR spectra of peroxidases reveal, in the high frequency region, marker bands sensitive to the spin, oxidation and coordination state of the haem iron.<sup>46, 47</sup> The spectra of BsDyP WT and variants indicate only subtle structural changes in the haem cavity brought up by the mutations, which are reflected in small

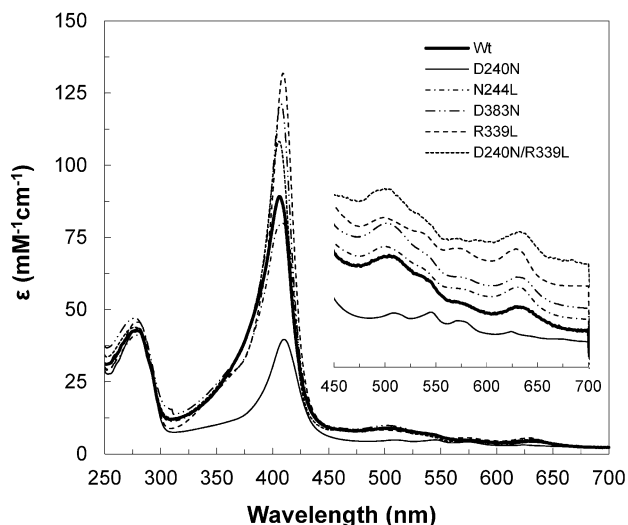


**Fig. 8** UV-visible spectra of BsDyP WT and variants (~2  $\mu\text{M}$  in 20 mM Tris-HCl at pH 7.6). The inset shows the region between 450 and 700 nm.

band shifts and changes of relative band intensities. Actually, RR spectra revealed that the effect of mutation is sensed by the active sites even in D383N and N244L, which carry the mutations furthest from the haem group.

The spin state sensitive  $\nu_3$  and  $\nu_2$  bands clearly indicate a presence of high spin (HS) and low spin (LS) species in the spectra of all studied variants (Fig. 9). Several spin populations, related to a high flexibility of the haem pocket in these enzymes, are commonly observed in RR spectra of bacterial and plant peroxidases, including

BsDyP, and PpDyP WT, as well as CcP, HRP and soybean peroxidase.<sup>47</sup> Furthermore, the frequencies as well as the relative intensities of the marker bands in the spectra of N244L, R339L, D383N and even D240N-R339L show remarkable similarities (only the D240N variant was insufficiently stable to allow for acquisition of spectra with sufficiently good signal to noise ratio). The spectral fingerprint of each of the four variants is distinct from that of the

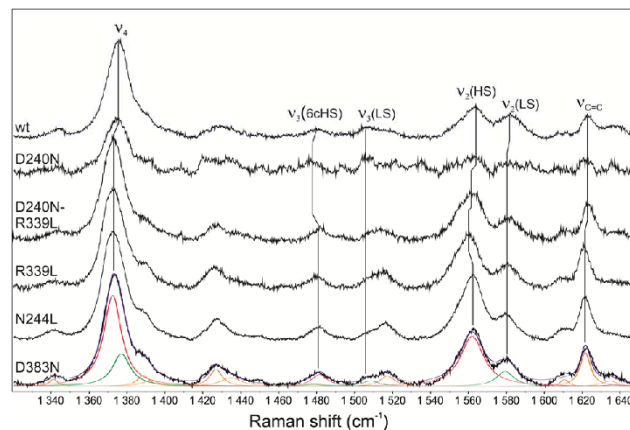


**Fig. 9** High frequency region of resonance Raman spectra of ferric BsDyP WT and D240N, D240N-R339L, R339L, N244L and D383N variants (top to bottom). The spectra of 10-50  $\mu\text{M}$  proteins in 50 mM Tris-HCl, pH 7.6 were measured with 413 nm excitation and 7 mW laser power at RT. The experimental spectrum of D383N (black trace) is shown together with its component spectra, representing 6cHS (red trace) and 6cLS (green trace) populations, non-assigned or spin-state insensitive bands (orange trace) and the overall fit (blue trace).

wild type, in particular with respect to the relative intensities of  $\nu_2$  (HS) vs.  $\nu_2$  (LS). Component analysis of the spectra confirmed the presence of two 6-coordinated populations in R339L ( $\nu_4$ ,  $\nu_3$  and  $\nu_2$  at 1371, 1481 and 1561  $\text{cm}^{-1}$  for 6cHS and 1377, 1507 and 1582  $\text{cm}^{-1}$  for 6cLS), N244L and D383N ( $\nu_4$ ,  $\nu_3$  and  $\nu_2$  at 1372, 1481 and 1569  $\text{cm}^{-1}$  for 6cHS and 1377, 1508 and 1582  $\text{cm}^{-1}$  for 6cLS) and the double mutant ( $\nu_4$ ,  $\nu_3$  and  $\nu_2$  at 1371, 1482 and 1562  $\text{cm}^{-1}$  for 6cHS and 1376, 1508 and 1581  $\text{cm}^{-1}$  for 6cLS), previously observed in the BsDyP WT.<sup>45, 46</sup> Quantification of the relative amount of these spin populations (Table S1), indicates that the WT, followed by R339L show the highest amount of LS population.

### Redox properties of BsDyP variants

The influence of mutations on the redox properties of the  $\text{Fe}^{3+}/\text{Fe}^{2+}$  couple in BsDyP was assessed by cyclic voltammetry. Although not directly involved in the catalytic cycle, it is considered that the molecular factors that determine the  $E^{0'}_{\text{Fe}^{3+}/\text{Fe}^{2+}}$  values also influence the catalytically relevant redox couples, *i.e.*  $\text{Fe}^{3+}/\text{Cpd I}$  and  $\text{Cpd I}/\text{Cpd II}$ .<sup>48, 49</sup> With the exception of D383N and N244L, the redox  $\text{Fe}^{3+}/\text{Fe}^{2+}$  transitions of variants undergo a substantial downshift with respect to the WT ( $E^{0'} = -40$  mV) (Table 1). The effect of altered H-bonding network caused by substitution of the polar, uncharged Asn for a non-polar Leu (of equivalent size) has a moderate impact on the redox potential of N244L variant as well as the substitution of the proximal aspartate by an asparagine (D383N) (Table 1). The moderate downshift of the redox potential of the proximal D383N is comparable to the lower  $E^{0'}_{\text{Fe}^{3+}/\text{Fe}^{2+}}$  of the D245N mutant in Class II

peroxidase from *Coprinus cinereus*.<sup>50</sup> The substitution of the distal aspartate residue (D240) by the asparagine, both in the single and the double mutant, decreased the  $E^0_{\text{Fe}^{3+}/\text{Fe}^{2+}}$  of BsDyP; the introduction of asparagine and glutamine residues in place of the distal histidine in classical peroxidases has a similar effect.<sup>48</sup> The D240N analogue in yeast CcP (H52N) also showed a large and negative shift of redox potential.<sup>51</sup> This was rationalized in terms of opening of the haem distal cavity in the presence of asparagine, which induced a reorganization of the hydrogen-bonding network and increased the accessibility of the haem group to solvent and, consequently, the polarity of the distal haem cavity.<sup>48</sup> These effects stabilize the ferric state which, according to Kassner,<sup>52</sup> can account for up to 200 mV decrease of the midpoint potential. The substitution of polar and charged distal Arg339 in BsDyP for less bulky and hydrophobic Leu also had a substantial impact on redox potential (~65 mV decrease).

### Reaction of BsDyP variants with hydrogen peroxide

The effect of distal and proximal mutations in the reaction of BsDyP with  $\text{H}_2\text{O}_2$  was probed by stopped flow measurements at pH 3.8–4.4 (Figs. S6 and S7) and at pH 7 (Figs. S8 and S9). Note that pH 4.4 is the optimal for D240N and D240N-R339L variants (Fig. S5). The obtained data reveal that N244L and D383N mutations lead to formation of a stable Cpd I intermediate similarly to WT at pH 3.8 (Figs. S6 and S7). In contrast, an unstable Cpd I was formed in variants D240N and R339L, which was spontaneously converted to Cpd II in acidic conditions. The double D240N-R339L variant, with simultaneous substitution of Asp and Arg residues, shows a rapid degradation of Cpd I upon its formation (Fig. S6 C). At pH 7, Cpd II follows Cpd I formation in all tested variants at rates comparable to the BsDyP WT (Figs. S8 and S9).

The  $\text{H}_2\text{O}_2$  concentration dependence of the initial rates ( $k_{1\text{obs}}$ ) of Cpd I formation at the optimal pH, shown in Fig. 10, demonstrated that all variants exhibited saturation kinetics, as observed in the WT enzyme (Fig. 3A). This behaviour can be explained by the reaction mechanism described in the kinetic scheme (1). The kinetic parameters for Cpd I formation by the variants (Table 2) were calculated using the equation (3). An increased apparent dissociation constant ( $K_1$ ) for  $\text{H}_2\text{O}_2$  as compared to WT was measured in all variants, indicating that substitution of distal residues and, to a lesser extent, of the proximal Asp, affects the first step of Cpd I formation. This step corresponds to the formation of  $\text{E-H}_2\text{O}_2$  *i.e.* deprotonation of the incoming hydrogen peroxide and binding of the peroxide anion to the Fe(III) haem.<sup>19, 27, 28</sup> The most pronounced effects in the  $K_1$  originate from individual substitutions of distal Asp and Arg residues that lead to ~60-fold (in D240N and R339L variants) and ~120-fold (in the D240N-R339L variant) higher values as compared with WT. These results point to a critical role of both residues in the proper coordination of  $\text{H}_2\text{O}_2$  at the haem of BsDyP. Interestingly, an opposite effect was observed in the first-order rate constant ( $k_1$ ) in D240N and R339L distal variants: a ~4-fold lower rate (than for the WT) upon substitution of D240 and a ~4-fold higher rate upon substitution of R339. This indicates a major role of distal Asp with respect to the stabilisation of the transient state for the O-O bond heterolytic cleavage in the second step of Cpd I formation. Importantly, a 25-fold lower rate is exhibited in the double D240N-

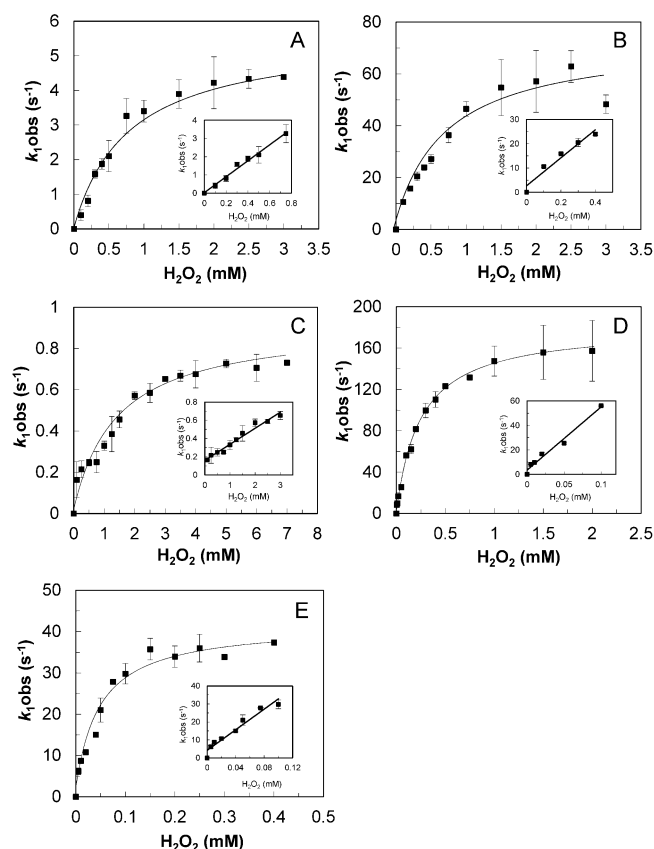


**Figure 10** – Dependence of  $k_{1\text{obs}}$  vs.  $[\text{H}_2\text{O}_2]$  in reactions of BsDyP variants: D240N and D240N-R339L at pH 4.4 (A, C) and R339L (B), N244L (D) and D383N (E) at pH 3.8. Cpd I formation was followed at 397 nm (Figs. S6 and S7).

R339L showing that the variant D240 apparently, requires the presence of the distal Arg residue for the full reactivity. The steady-state kinetics of  $\text{H}_2\text{O}_2$  reduction in the presence of ABTS (Table 3) reveals that D240N, R339L and D240N-R339L variants, show the lowest catalytic efficiency ( $k_{\text{cat}}/K_m$ ) among the variants, with two- (D240N and R339L) to three- (D240N-R339L) orders of magnitude lower values as compared to WT. The decreased efficiency of these distal variants is mostly due to the  $K_m$  term which is 50- to 400-fold higher as compared to the WT enzyme, in good agreement with the kinetic parameters measured in the stopped-flow experiments. Interestingly, none of the variants shows inhibition by increasing concentrations of hydrogen peroxide (Fig. S10) as observed for WT BsDyP ( $K_i$  of 0.2 mM for  $\text{H}_2\text{O}_2$ ).<sup>12</sup>

The substitution of the distal N244 residue shows a lower impact on the accessibility of hydrogen peroxide to the distal pocket as compared with substitution of D240 and R339 considering the 10-fold higher  $K_1$  constant of the WT (Table 2). Surprisingly, the N244L variant is highly reactive towards hydrogen peroxide showing a 10-fold higher rate constant and approximately only one-order lower  $k_{\text{cat}}/K_m$  than the WT (Table 2 and 3). Considering the relatively small differences in the rate constants observed in the D240N variant as compared to the WT, it seems reasonable to speculate that Asn244 and surrounding residues can at least partially compensate for the absence of Asp in the acid-base mechanism of BsDyP. Distal Asn244 is 4 and 7 Å apart from Arg339 and Asp240, respectively,

**Table 2.** Kinetic parameters for the formation of the Cpd I ( $K_1$ ,  $k_1$ ) and Cpd II ( $k_2$ ) in the reaction of variants with  $H_2O_2$  at respective optimal pH, determined from stopped-flow experiments. The kinetic parameters are the median of the values obtained from at least six independent traces.

	$K_1$ ( $\times 10^{-6}$ M)	$k_1$ ( $s^{-1}$ )	$k_2$ ( $s^{-1}$ )
WT	12 $\pm$ 1	22 $\pm$ 1	-
D240N	795 $\pm$ 112	5.8 $\pm$ 0.3	3 $\pm$ 1
R339L	714 $\pm$ 161	74 $\pm$ 6	9 $\pm$ 1
D240N-R339L	1413 $\pm$ 229	0.9 $\pm$ 0.1	- <sup>a</sup>
N244L	246 $\pm$ 14	179 $\pm$ 3	-
D383N	49 $\pm$ 7	43 $\pm$ 2	-

nd- not determined.

<sup>a</sup> Protein degradation was observed.

in the BsDyP model structure.<sup>12</sup> Moreover, the X-ray structure of *R. jostii* RHA1 DyPB indicates that the conserved Asn246 and Asp153 are hydrogen bonded to a shared solvent molecule, contributing both to the electrostatic environment and the hydrogen bonding network of the active site; additionally, their synergistic action in the peroxidase activity was suggested by the analysis of the D153A-N246A double variant.<sup>17</sup> As expected, the proximal D383N substitution has the smallest impact on the accessibility of hydrogen peroxide to the distal pocket of BsDyP and on the kinetics of Cpd I formation (Tables 2 and 3).

**Table 3.** Apparent steady-state catalytic parameters for  $H_2O_2$  (0.001 - 2 mM for WT, D240N, D240N-R339L and D383N; 0.001 - 8 mM for R339L and N244L), determined at 25°C, in 20 mM sodium acetate buffer at respective optimal pH using ABTS as substrate (0.2 mM for R339L and 1 mM for WT, D240N, N244L, D240N-R339L and D383N).

	$K_m$ ( $\mu$ M)	$k_{cat}$ ( $s^{-1}$ )	$k_{cat}/K_m$ ( $M^{-1}s^{-1}$ )
WT*	7 $\pm$ 1	12 $\pm$ 3	2 $\times 10^6$
D240N	362 $\pm$ 64	11 $\pm$ 1	3 $\times 10^4$
R339L	1082 $\pm$ 44	46 $\pm$ 12	4 $\times 10^4$
D240N-R339L	2736 $\pm$ 348	2.3 $\pm$ 0.2	1 $\times 10^3$
N244L	545 $\pm$ 68	138 $\pm$ 5	3 $\times 10^5$
D383N	56 $\pm$ 7	17 $\pm$ 1	3 $\times 10^5$

\* 12

Overall, the data reveal an important, but apparently not crucial role, of either individual Asp or Arg in the catalytic mechanism of BsDyP. Furthermore, our kinetic data point out to the involvement of distal Asn, in addition to Asp and Arg, in modulating the acid-base catalysis of the BsDyP. The compromised activity in both D240N and R339L variants reflects only 2 to 3-orders of magnitude decreased efficiency, far from that observed in HRP and CcP variants, in which distal residue substitutions results in 5-6 orders of magnitude decreased rate of Cpd I formation.<sup>19, 33</sup> Furthermore, our data cannot support either the results reported on D type *B. adusta* Dec I DyP in which no spectral changes were observed in D171N variant upon addition of peroxide<sup>16, 23</sup> or those on B type *R. jostii*

RHA1 DyPB or *P. putida* MET94 PpDyP, where substitution of distal Arg leads to the absence or severely compromised catalytic activity, respectively.<sup>17, 41</sup> In BsDyP, the positively charged guanidinium group of the Arg339 most likely has a role in both orientation of the hydrogen peroxide at the active centre and in promoting the heterolytic cleavage of peroxide as proposed in HRP.<sup>33, 34</sup> The distal Asp240 can, on the other hand, acts as a proton acceptor from the incoming hydrogen peroxide, facilitating the binding of the peroxide anion to the haem and assisting the heterolytic cleavage of the oxygen-oxygen bond. This is supported by the observed pH dependence of rate of Cpd I formation (Fig. 4) and the (0.6 unit) increased optimal pH measured in D240N and D240N-R339L variants (Fig. S5). This presumably involves the proton donation by either residue to the  $\beta$ -oxygen of the bound peroxide anion thereby promoting the elimination of  $H_2O$ . One hypothesis is that the redox potential of the WT BsDyP ( $E^0 = -40$  mV) and variants D240N ( $E^0 = -120$  mV) and R339L ( $E^0 = -105$  mV), substantially higher than those reported for the majority of other peroxidases,<sup>45, 49</sup> may lower the  $pK_a$  of hydrogen peroxide upon binding to the haem molecule, and facilitate its (de)protonation by the Asp or protonation by the Arg residues, that act synergistically with respect to peroxide O-O bond cleavage.

#### Reaction of BsDyP variants with reducing substrates

Unexpectedly, the analysis of the kinetic data for bulkier oxidizing substrates reveals that the substitution of distal and proximal residues leads to either similar or increased catalytic efficiency as compared to the WT (Table 4 and Fig. S10). Again, the altered efficiency is mostly due to the  $K_m$  term since significantly lower  $K_m$  values were measured for all distal variants. However, comparable or improved turnover numbers ( $k_{cat}$ ) in respect to those reported for the WT were observed in all cases (Table 4). For example, R339L variant shows around 3 to 10 times lower  $K_m$  and  $\sim 5$ -fold higher rates for guaiacol and ABTS, respectively, which resulted in increased efficiencies of 1 to 2-orders of magnitude for these substrates as compared with the WT. It is noteworthy that N244L exhibits 7 to 20 times higher catalytic rates and slightly lower  $K_m$  values for all tested substrates, showing catalytic efficiencies that are 1 to 2-orders of magnitude higher in comparison with that of the WT enzyme. As demonstrated for the reduction of  $H_2O_2$ , we can conclude that none of the studied variants shows a compromised catalytic efficiency towards the tested substrates. But, as observed before for  $H_2O_2$ , the variant that performs worst is D240N. The substrate oxidation site is often unknown in haem peroxidases. A surface exposed and conserved Tyr/Trp residues were shown to be involved in peripheral substrate oxidation in *Auricularia auriculae-judae* AauDyPI, required for the long range electron transfer pathway from the redox active amino acid residue to the porphyrin ring, comparable to those described in lignin, versatile or manganese peroxidases.<sup>15, 53, 54</sup> Importantly, in the fungal AauDyPI distal Asp-168 was proposed to act as a gatekeeper by altering the width of the haem access channel, enabling the enzyme to oxidize substrates larger than  $H_2O_2$  directly inside the haem cavity.<sup>53</sup> According to this view, we can hypothesize that the conformational alterations that result from the substitution of distal residues in BsDyP allow bulkier substrates to be oxidized with an apparent improved

**Table 4.** Apparent steady-state catalytic parameters of WT BsDyP and variants measured at 25°C in 20 mM sodium acetate buffer at optimal pH for the enzymes (pH 3.8 for WT, R339L, N244L and D383N and at pH 4.4 for D240N and D240N-R339L) under conditions described in the Experimental section.

	$K_m$ ( $\mu\text{M}$ )					
	WT*	D240N	R339L	D240N/R339L	N244L	D383N
ABTS	166 ± 14	48 ± 10	14 ± 7	11 ± 3	48 ± 4	321 ± 53
Acid blue 62	444 ± 45	262 ± 71	104 ± 18	- <sup>a</sup>	162 ± 27	384 ± 62
Mordant black 9	385 ± 46	94 ± 8	18 ± 4	- <sup>a</sup>	241 ± 37	63 ± 9
Guaiacol	86 ± 15	172 ± 40	27 ± 9	- <sup>a</sup>	258 ± 63	27 ± 7
Mn <sup>2+</sup>	40 ± 7	- <sup>a</sup>	- <sup>a</sup>	- <sup>a</sup>	54 ± 9	- <sup>a</sup>
	$k_{\text{cat}}$ ( $\text{s}^{-1}$ )					
	WT*	D240N	R339L	D240N/R339L	N244L	D383N
ABTS	11 ± 1	13 ± 1	40 ± 4	3.0 ± 0.2	98 ± 2	15 ± 1
Acid Blue 62	9.1 ± 0.2	24 ± 3	14 ± 1	- <sup>a</sup>	203 ± 14	36 ± 4
Mordant Black 9	3.8 ± 0.1	1.5 ± 0.1	5.3 ± 0.3	- <sup>a</sup>	30 ± 2	3.0 ± 0.1
Guaiacol	0.12 ± 0.01	0.08 ± 0.01	0.7 ± 0.1	- <sup>a</sup>	1.1 ± 0.1	0.15 ± 0.01
Mn <sup>2+</sup>	0.30 ± 0.02	0.15 ± 0.01	0.23 ± 0.04	- <sup>a</sup>	5.3 ± 0.2	0.23 ± 0.02
	$k_{\text{cat}}/K_m$ ( $\text{M}^{-1}\text{s}^{-1}$ )					
	WT*	D240N	R339L	D240N/R339L	N244L	D383N
ABTS	7 × 10 <sup>4</sup>	3 × 10 <sup>5</sup>	3 × 10 <sup>6</sup>	3 × 10 <sup>5</sup>	2 × 10 <sup>6</sup>	5 × 10 <sup>4</sup>
Acid Blue 62	2 × 10 <sup>4</sup>	1 × 10 <sup>5</sup>	1 × 10 <sup>5</sup>	- <sup>a</sup>	1 × 10 <sup>6</sup>	1 × 10 <sup>5</sup>
Mordant Black 9	1 × 10 <sup>4</sup>	2 × 10 <sup>4</sup>	3 × 10 <sup>5</sup>	- <sup>a</sup>	1 × 10 <sup>5</sup>	2 × 10 <sup>4</sup>
Guaiacol	1 × 10 <sup>3</sup>	1 × 10 <sup>3</sup>	9 × 10 <sup>3</sup>	- <sup>a</sup>	4 × 10 <sup>3</sup>	1 × 10 <sup>4</sup>
Mn <sup>2+</sup>	1 × 10 <sup>4</sup>	- <sup>a</sup>	- <sup>a</sup>	- <sup>a</sup>	1 × 10 <sup>5</sup>	- <sup>a</sup>

\* 12

<sup>a</sup>- Not determined

efficiency in the close vicinity of the haem. Our data point in particular to the importance of substitution of R339 for a smaller residue in facilitating the substrate access to the haem. A more complete understanding of the binding sites for compounds important in biotechnology is of crucial importance in order to be able to exploit BsDyP and other bacterial DyPs for industrial applications.

## Experimental

### Construction, overproduction and purification of BsDyP variants

Single amino acid substitutions were created using the QuickChange site-directed mutagenesis kit (Stratagene). Plasmid pRC-2 (containing the wild-type (WT) *bsDyP* sequence) was used as template<sup>12</sup>. The primers, forward 5'-GATGGAACAGGCCTGCAGAGCACGAAGGATGACACG-3' and reverse 5'-CGTGTTCATCCTTCGTGCTCTGCAGGCCTGTTCCATC-3' were used to create N244L mutation; forward 5'-CCTCTTCGGGTTTAAAAACGGAACAGGCAACCAG-3' and reverse 5'-CTGGTTGCCTGTTCCGTTTTTAAACCCGAAGAGG-3' for D240N mutation; forward 5'-GGCTCTTTCAGCAAAGAACGCGTTAAACGAATATAC-3' and reverse 5'-

GTATATTCGTTTAAACGCGTTCTTTGCTGAAAGAGCC-3' for D383N mutation; forward 5'-GGGAAACAAATTTTGCTGAGAGCTTCTCTTAC-3' and reverse 5'-GTAAGAGAAAGCTCTCAGCAAATTTGTTTCCC-3' for R339L mutation. Plasmid carrying the D240N point mutation was used as a template and the forward 5'-GGGAAACAAATTTTGCTGAGAGCTTCTCTTAC-3' and reverse 5'-GTAAGAGAAAGCTCTCAGCAAATTTGTTTCCC-3' primers were used to generate the double mutant D240N-R339L. The presence of the desired mutation in the resulting plasmids and the absence of unwanted mutations in other regions of the insert were confirmed by DNA sequence analysis. The plasmids containing the *bsDyP* gene with the desired mutations were transformed into *Escherichia coli* BL21-star strain, in which the recombinant BsDyP variants were produced under the control of the *T7lac* promoter. Cell growth, disruption and protein purification were undertaken as previously described.<sup>12</sup> The protein concentration was determined by the Bradford assay with bovine serum albumin as standard. Purified enzymes were stored at -20°C until use.

### Spectroscopic analysis

The UV-visible absorption spectra of purified enzymes were recorded on a Nicolet Evolution 300 spectrophotometer (Thermo Industries). The Reinheitszahl values were determined by the ratio between absorbance at the wavelength of the Soret band and absorbance at 280 nm ( $A_{\text{Soret}}/A_{280\text{nm}}$ ). The haem content was determined by the pyridine ferro-hemochrome method using the

extinction coefficient of pyridine hemochromes (R) minus the extinction coefficient of pyridine hemichrome (O), ( $\epsilon_{R-O}$ ) at 556 nm ( $28.32 \text{ mM}^{-1}\text{cm}^{-1}$ ).<sup>55</sup> Room temperature resonance Raman experiments were carried out in a rotating cuvette (from Hellma) containing  $\sim 80 \mu\text{L}$  of 10 - 50  $\mu\text{M}$  sample in 50 mM Tris-HCl, pH 7.6, to prevent prolonged exposure of individual enzyme molecules to laser irradiation. The laser power was set to 7 mW; 10 spectra, measured with 60 s accumulation times were co-added in each measurement. All spectra were subjected to polynomial baseline subtraction and component analysis as described previously using in-house made software.<sup>45,56</sup>

### Cyclic Voltammetry

Electrochemical measurements were carried out in a three-electrode cell containing a working pyrolytic graphite electrode (basal plane), a platinum wire counter electrode and a Ag/AgCl reference electrode. The supporting electrolyte, 0.1 M KCl in 50 mM Tris-HCl pH 7.6 was thoroughly purged with argon before each experiment. The cyclic voltammetry measurements were performed using a Princeton Applied Research 263A potentiostat. The potential was cycled between 0.1 and -0.7 V vs. Ag/AgCl at scan rates between 20 and 150  $\text{mVs}^{-1}$ . Prior to each experiment, the working electrode was polished with alumina slurry (0.3  $\mu\text{m}$  particle size), thoroughly washed with water, ultrasonicated for 5 min and dried with compressed air. A small volume of the protein solution ( $\sim 10 \mu\text{L}$  of 5 - 10  $\mu\text{M}$  protein in 50 mM Tris-HCl, pH 7.6) was entrapped between the electrode surface and a dialysis membrane (MWCO 3000, Spectra/Por), which was fixed around the electrode body by a rubber o-ring.<sup>57</sup>

### Stopped-flow experiments

Transient state kinetics were studied by mixing protein solutions with  $\text{H}_2\text{O}_2$  or guaiacol in a Hi-Tech SF-61DX2 stopped-flow apparatus coupled to a diode array for signal detection. A circulating water bath was used to maintain the temperature of the reactant syringes and the mixing cell at 25°C. 2  $\mu\text{M}$  of enzyme was mixed with 0-50  $\mu\text{M}$   $\text{H}_2\text{O}_2$  (WT), 0-400  $\mu\text{M}$   $\text{H}_2\text{O}_2$  (D383N) and 0-2000  $\mu\text{M}$   $\text{H}_2\text{O}_2$  (N244L); 4  $\mu\text{M}$  of enzyme was mixed with 0-3000  $\mu\text{M}$   $\text{H}_2\text{O}_2$  (D240N and R339L) and 0-7000  $\mu\text{M}$   $\text{H}_2\text{O}_2$  (D240N-R339L). The  $\text{H}_2\text{O}_2$  equivalents when mentioned are in relation to the holoprotein fraction of the enzyme preparation i.e. in relation to the haem content of the protein preparation and not the total protein content. All concentrations referred in the text are after mixing. UV-Vis spectra (350 - 700 nm) were recorded at different time scales in the pH range of 3-9 using BR buffer (100 mM phosphoric acid, 100 mM boric acid, and 100 mM acetic acid mixed with NaOH to the desired pH). The concentration of the protein solutions was determined from the absorbance at  $\lambda = 280 \text{ nm}$  using the extinction coefficient  $\epsilon_{280\text{nm}} = 42,650 \text{ M}^{-1}\text{cm}^{-1}$ , calculated from the protein sequence using the ExpASY Bioinformatics Resource Portal (<http://web.expasy.org>). The  $\text{H}_2\text{O}_2$  solutions were prepared from successive dilutions of a stock solution;  $\lambda = 240 \text{ nm}$  ( $\epsilon_{240\text{nm}} = 39.4 \text{ M}^{-1}\text{cm}^{-1}$ ).<sup>58</sup> The rate constants for Cpd I formation ( $k_{1\text{obs}}$ ) were obtained from the exponential fit of the absorbance decrease measured at 397 nm, a wavelength where the possible subsequent formation of Cpd II did not interfere in the measurement (Fig. S1). The first order rate

constants ( $k_1$  ( $\text{s}^{-1}$ )) and the apparent dissociation constants ( $K_1$  (M)) were obtained by fitting the equation (3) to the data. The first order rate constant of the second step  $k_2$  (when Cpd I decayed to Cpd II intermediate), was obtained directly from the exponential fit of the absorbance measured at 420 nm, the isosbestic point between resting BsDyP and variants and Cpd I (Fig. S1). The half-life ( $t_{1/2}$ ) of WT Cpd I was determined using the equation  $t_{1/2} = \ln 2/k$ , where  $k$  is the rate constant calculated as the slope of the line defined by the linear regression of the natural logarithm of the decrease of absorbance at 397 nm (for Cpd I) as a function of time. The rate constants for BsDyP WT at pH 3.8 for Cpd II formation ( $k_{3\text{obs}}$ ) and its subsequent conversion to the resting enzyme ( $k_{4\text{obs}}$ ) in the presence of guaiacol as reducing substrate were obtained from the exponential fit of the absorbance increase and subsequent decrease measured at 420 nm in the presence of increasing concentrations of guaiacol. In these experiments BsDyP WT with 2 equivalents of  $\text{H}_2\text{O}_2$  was mixed with guaiacol. The second order rate constant  $k_3'$  (when Cpd I decayed to Cpd II in the presence of guaiacol) was obtained from the slope of the plot  $k_{3\text{obs}}$  vs. [guaiacol]. The first order rate constant ( $k_4$  ( $\text{s}^{-1}$ )) and the apparent dissociation constant ( $K_4$  (M)) were obtained by fitting equation (8) to the data.

### Steady-state kinetic assays

The enzymatic activity of BsDyP WT and variants was monitored using either a Nicolet Evolution 300 spectrophotometer (Thermo Industries), or a Synergy2 microplate reader (BioTek). The holoprotein concentration was considered for the measurement of the specific activity of BsDyP WT and variants. All enzymatic assays were performed at least in triplicate. The activity dependence on pH was measured by monitoring the oxidation of 1 mM ABTS at 420 nm ( $\epsilon_{420\text{nm}} = 36,000 \text{ M}^{-1}\text{cm}^{-1}$ ) in the presence of 0.2 mM  $\text{H}_2\text{O}_2$  at 25°C using BR buffer (pH in the range of 2 - 7). All enzymatic assays were performed at 25°C, in 20 mM sodium acetate buffer at optimal pH for each of the enzymes (pH 3.8 for WT, R339L, N244L and D383N and pH 4.4 for D240N and D240N-R339L variants). The apparent steady-state kinetic parameters for  $\text{H}_2\text{O}_2$  (0.001 - 2 mM for WT, D240N, D240N-R339L and D383N; 0.001 - 8 mM for R339L and N244L) using ABTS as substrate (0.2 mM for R339L and 1 mM for WT, D240N, N244L, D240N-R339L and D383N) and adequate amounts of respective enzymes. The apparent steady-state kinetic parameters were measured for ABTS (0.05 - 2 mM) with 0.2 mM  $\text{H}_2\text{O}_2$  for WT, 1 mM for D383N, D240N and D240N-R339L and 5 mM for R339L and N244L and adequate amounts of the respective enzyme. Apparent steady-state kinetic parameters were measured for guaiacol ( $\epsilon_{470\text{nm}} = 26,600 \text{ M}^{-1}\text{cm}^{-1}$ ) (0.01 - 2 mM), acid blue 62 (AB62) ( $\epsilon_{600\text{nm}} = 10,920 \text{ M}^{-1}\text{cm}^{-1}$ ) (0.01 - 1 mM), and mordant black 9 (MB9) ( $\epsilon_{550\text{nm}} = 15,641 \text{ M}^{-1}\text{cm}^{-1}$ ) (0.01 - 2 mM) using the  $\text{H}_2\text{O}_2$  concentrations described above at the optimal pH for each variant. A discontinuous assay was used in the reaction of WT with acid blue 62 for concentrations above 0.5 mM (exhibiting values out of the Lambert-Beer law's applicability range), where samples were withdrawn from reactions at specific time intervals, diluted with buffer and the absorbance measured at 600 nm. Reactions with  $\text{MnCl}_2$  were performed in 50 mM sodium lactate and  $\text{Mn}^{3+}$ -lactate formation was monitored at 270 nm ( $\epsilon_{270\text{nm}} = 3,500 \text{ M}^{-1}\text{cm}^{-1}$ ) (0.05-2 mM) using the  $\text{H}_2\text{O}_2$  concentrations described above

at the optimal pH for each variant. The apparent kinetic parameters  $k_{\text{cat}}$  and  $K_m$  were obtained by fitting the data using the Michaelis-Menten equation (Origin-Lab software).

## Conclusions

In conclusion, we have elucidated the catalytic cycle of BsDyP at pH 3.8 and pH 7 and have provided the first kinetic evidence for the formation of a reversible enzyme-H<sub>2</sub>O<sub>2</sub> complex (Compound 0) which was previously observed only at sub-zero temperatures using cryosolvents.<sup>29-32, 35</sup> We show that Cpd I formation in the reaction of BsDyP and H<sub>2</sub>O<sub>2</sub> is strongly pH dependent as well as its spontaneous decay to Cpd II. The kinetic analysis of the reaction of guaiacol with Cpd I and Cpd II demonstrates the formation of a pre-equilibrium binding of guaiacol to Cpd II prior to rate-limiting electron transfer, which constitutes the limiting step in the overall BsDyP catalytic cycle. Importantly, by combining electrochemical, spectroscopic and kinetic approaches, we demonstrate that none of the conserved distal residues in BsDyP appears to be indispensable for promoting the (de)protonation of H<sub>2</sub>O<sub>2</sub> and the cleavage of the O-O bond. These findings are in clear contrast with previous data derived from site-directed mutagenesis studies of several DyPs, which have suggested that either the conserved Asp or the Arg plays the key role in catalysis, guiding the hydrogen peroxide toward the haem iron, mediating the proton rearrangement and heterolytic cleavage of dioxygen.<sup>15-18, 23</sup> Moreover, our studies suggest an important role of distal Asn in modulating the acid-base catalysis of BsDyP. This study will in particular contribute to establishing whether the differences in mechanistic features of DyPs are related to functionally diverse enzymes from different sources, or a consistent mechanistic model can be constructed for this peroxidase family, after a sufficiently large body of experimental evidence becomes available.

## Acknowledgements

The authors thank D. Presa for assistance in preliminary studies and D. L. Turner for helpful discussions. This work was supported by Fundação para a Ciência e Tecnologia, Portugal; Grants: PEst-OE/UI0100/2013, EXP/BBB-BIO/1932/2013 and Research Unit GREEN-it "Bioresources for Sustainability" (UID/Multi/04551/2013).

## References

- M. Hofrichter, R. Ullrich, M. J. Pecyna, C. Liers and T. Lundell, *Appl Microbiol Biotechnol*, 2010, **87**, 871-897.
- D. I. Colpa, M. W. Fraaije and E. van Bloois, *J Ind Microbiol Biotechnol*, 2014, **41**, 1-7.
- D. Linde, F. J. Ruiz-Duenas, E. Fernandez-Fueyo, V. Guallar, K. E. Hammel, R. Pogni and A. T. Martinez, *Arch Biochem Biophys*, 2015, **574**, 66-74.
- T. Yoshida and Y. Sugano, *Arch Biochem Biophys*, 2015, **574**, 49-55.
- R. Singh and L. D. Eltis, *Arch Biochem Biophys*, 2015, **574**, 56-65.
- D. Salvachua, A. Prieto, A. T. Martinez and M. J. Martinez, *Appl Environ Microbiol*, 2013, **79**, 4316-4324.
- R. Singh, J. C. Grigg, W. Qin, J. F. Kadla, M. E. Murphy and L. D. Eltis, *ACS Chem Biol*, 2013, **8**, 700-706.
- S. S. Adav, C. S. Ng, M. Arulmani and S. K. Sze, *J Proteome Res*, 2010, **9**, 3016-3024.
- M. Ahmad, J. N. Roberts, E. M. Hardiman, R. Singh, L. D. Eltis and T. D. Bugg, *Biochemistry*, 2011, **50**, 5096-5107.
- K. Min, G. Gong, H. M. Woo, Y. Kim and Y. Um, *Sci Rep*, 2015, **5**, 8245.
- Y. Sugano, *Cell Mol Life Sci*, 2009, **66**, 1387-1403.
- A. Santos, S. Mendes, V. Brissos and L. O. Martins, *Appl Microbiol Biotechnol*, 2014, **98**, 2053-2065.
- C. Zubieta, R. Joseph, S. S. Krishna, D. McMullan, M. Kapoor, H. L. Axelrod, M. D. Miller, P. Abdubek, C. Acosta, T. Astakhova, D. Carlton, H. J. Chiu, T. Clayton, M. C. Deller, L. Duan, Y. Elias, M. A. Elsliger, J. Feuerhelm, S. K. Grzechnik, J. Hale, G. W. Han, L. Jaroszewski, K. K. Jin, H. E. Klock, M. W. Knuth, P. Kozbial, A. Kumar, D. Marciano, A. T. Morse, K. D. Murphy, E. Nigoghossian, L. Okach, S. Oommachen, R. Reyes, C. L. Rife, P. Schimmel, C. V. Trout, H. van den Bedem, D. Weekes, A. White, Q. Xu, K. O. Hodgson, J. Wooley, A. M. Deacon, A. Godzik, S. A. Lesley and I. A. Wilson, *Proteins*, 2007, **69**, 234-243.
- C. Zubieta, S. S. Krishna, M. Kapoor, P. Kozbial, D. McMullan, H. L. Axelrod, M. D. Miller, P. Abdubek, E. Ambing, T. Astakhova, D. Carlton, H. J. Chiu, T. Clayton, M. C. Deller, L. Duan, M. A. Elsliger, J. Feuerhelm, S. K. Grzechnik, J. Hale, E. Hampton, G. W. Han, L. Jaroszewski, K. K. Jin, H. E. Klock, M. W. Knuth, A. Kumar, D. Marciano, A. T. Morse, E. Nigoghossian, L. Okach, S. Oommachen, R. Reyes, C. L. Rife, P. Schimmel, H. van den Bedem, D. Weekes, A. White, Q. Xu, K. O. Hodgson, J. Wooley, A. M. Deacon, A. Godzik, S. A. Lesley and I. A. Wilson, *Proteins*, 2007, **69**, 223-233.
- E. Strittmatter, C. Liers, R. Ullrich, S. Wachter, M. Hofrichter, D. A. Plattner and K. Piontek, *J Biol Chem*, 2013, **288**, 4095-4102.
- T. Yoshida, H. Tsuge, H. Konno, T. Hisabori and Y. Sugano, *FEBS J*, 2011, **278**, 2387-2394.
- R. Singh, J. C. Grigg, Z. Armstrong, M. E. Murphy and L. D. Eltis, *J Biol Chem*, 2012, **287**, 10623-10630.
- X. Liu, Q. Du, Z. Wang, D. Zhu, Y. Huang, N. Li, T. Wei, S. Xu and L. Gu, *J Biol Chem*, 2011, **286**, 14922-14931.
- A. N. Hiner, E. L. Raven, R. N. Thorneley, F. Garcia-Canovas and J. N. Rodriguez-Lopez, *J Inorg Biochem*, 2002, **91**, 27-34.
- T. L. Poulos, *Arch Biochem Biophys*, 2010, **500**, 3-12.
- M. E. Brown, T. Barros and M. C. Chang, *ACS Chem Biol*, 2012, **7**, 2074-2081.
- J. N. Roberts, R. Singh, J. C. Grigg, M. E. Murphy, T. D. Bugg and L. D. Eltis, *Biochemistry*, 2011, **50**, 5108-5119.
- Y. Sugano, R. Muramatsu, A. Ichiyanaagi, T. Sato and M. Shoda, *J Biol Chem*, 2007, **282**, 36652-36658.
- T. Yoshida, H. Tsuge, T. Hisabori and Y. Sugano, *FEBS Lett*, 2012, **586**, 4351-4356.
- D. Linde, R. Pogni, M. Canellas, F. Lucas, V. Guallar, M. C. Baratto, A. Sinicropi, V. Saez-Jimenez, C. Coscolin, A. Romero, F. J. Medrano, F. J. Ruiz-Duenas and A. T. Martinez, *Biochem J*, 2015, **466**, 253-262.
- E. van Bloois, D. E. Torres Pazmino, R. T. Winter and M. W. Fraaije, *Appl Microbiol Biotechnol*, 2010, **86**, 1419-1430.
- T. L. Poulos and J. Kraut, *J Biol Chem*, 1980, **255**, 8199-8205.

28. P. Jones and H. B. Dunford, *J Inorg Biochem*, 2005, **99**, 2292-2298.
29. C. Balny, F. Travers, T. Barman and P. Douzou, *Eur Biophys J*, 1987, **14**, 375-383.
30. H. K. Baek and H. E. Van Wart, *J Am Chem Soc*, 1992, **114**, 718-725.
31. I. G. Denisov, T. M. Makris and S. G. Sligar, *J Biol Chem*, 2002, **277**, 42706-42710.
32. M. Tanaka, K. Matsuura, S. Yoshioka, S. Takahashi, K. Ishimori, H. Hori and I. Morishima, *Biophys J*, 2003, **84**, 1998-2004.
33. J. N. Rodriguez-Lopez, A. T. Smith and R. N. Thorneley, *J Biol Chem*, 1996, **271**, 4023-4030.
34. J. N. Rodriguez-Lopez, A. T. Smith and R. N. Thorneley, *J Biol Inorg Chem*, 1996, **1**, 136-142.
35. P. J. Mak, W. Thammawichai, D. Wiedenhoef and J. R. Kincaid, *J Am Chem Soc*, 2015, **137**, 349-361.
36. S. Nagano, M. Tanaka, K. Ishimori, Y. Watanabe and I. Morishima, *Biochemistry*, 1996, **35**, 14251-14258.
37. H. Wariishi, H. B. Dunford, I. D. MacDonald and M. H. Gold, *J Biol Chem*, 1989, **264**, 3335-3340.
38. L. Marquez, H. Wariishi, H. B. Dunford and M. H. Gold, *J Biol Chem*, 1988, **263**, 10549-10552.
39. M. Perez-Boada, F. J. Ruiz-Duenas, R. Pogni, R. Basosi, T. Choinowski, M. J. Martinez, K. Piontek and A. T. Martinez, *J Mol Biol*, 2005, **354**, 385-402.
40. H. B. Dunford and J. S. Stillman, *Coord Chem Rev*, 1976, 187-251.
41. S. Mendes, V. Brissos, A. Gabriel, T. Catarino, S. Todorovic and L. O. Martins, *Arch Biochem Biophys*, 2015, **574**, 99-107.
42. H. Wariishi, J. Huang, H. B. Dunford and M. H. Gold, *J Biol Chem*, 1991, **266**, 20694-20699.
43. J. N. Rodriguez-Lopez, M. A. Gilabert, J. Tudela, R. N. Thorneley and F. Garcia-Canovas, *Biochemistry*, 2000, **39**, 13201-13209.
44. A. K. Abelskov, A. T. Smith, C. B. Rasmussen, H. B. Dunford and K. G. Welinder, *Biochemistry*, 1997, **36**, 9453-9463.
45. M. Sezer, A. Santos, P. Kielb, T. Pinto, L. O. Martins and S. Todorovic, *Biochemistry*, 2013, **52**, 3074-3084.
46. F. Siebert and P. Hildebrandt, *Vibrational Spectroscopy in Life Sciences*, Wiley-VCH Verlag GmbH & Co. Weinheim Germany, 2008.
47. G. Smulevich, A. Feis and B. D. Howes, *Acc Chem Res*, 2005, **38**, 433-440.
48. G. Battistuzzi, M. Bellei, C. A. Bortolotti and M. Sola, *Arch Biochem Biophys*, 2010, **500**, 21-36.
49. M. Ayala, in *Biocatalysis based on heme peroxidases*, eds. E. Torres and M. Ayala, Springer Berlin Heidelberg, 2010, pp. 61-44.
50. C. Ciaccio, A. Rosati, G. De Sanctis, F. Sinibaldi, S. Marini, R. Santucci, P. Ascenzi, K. G. Welinder and M. Coletta, *J Biol Chem*, 2003, **278**, 18730-18737.
51. C. M. DiCarlo, L. B. Vitello and J. E. Eрман, *J Inorg Biochem*, 2007, **101**, 603-613.
52. R. J. Kassner, *J Am Chem Soc*, 1973, **95**, 2674-2677.
53. E. Strittmatter, S. Wachter, C. Liers, R. Ullrich, M. Hofrichter, D. A. Plattner and K. Piontek, *Arch Biochem Biophys*, 2013, **537**, 161-167.
54. E. Strittmatter, K. Serrer, C. Liers, R. Ullrich, M. Hofrichter, K. Piontek, E. Schleicher and D. A. Plattner, *Arch Biochem Biophys*, 2015, **574**, 75-85.
- E. A. Berry and B. L. Trumpower, *Anal Biochem*, 1987, **161**, 1-15.
- M. Sezer, T. Genebra, S. Mendes, L. O. Martins and S. Todorovic, *Soft Matter*, 2012, **8**, 10314-10321.
- J. Haladjian, I. Thierry-Chef and P. Bianco, *Talanta*, 1996, **43**, 1125-1130.
- D. P. Nelson and L. A. Kiesow, *Anal Biochem*, 1972, **49**, 474-478.